

## Spin dynamics and level structure of quantum-dot quantum wells

Jesse Berezovsky, Min Ouyang, Florian Meier, and David D. Awschalom

*Center for Spintronics and Quantum Computation, University of California, Santa Barbara, California 93106, USA*

David Battaglia and Xiaogang Peng

*Department of Chemistry and Biochemistry, University of Arkansas, Fayetteville, Arkansas 72701, USA*

(Received 5 November 2004; revised manuscript received 13 December 2004; published 23 February 2005)

We have characterized CdS/CdSe/CdS quantum-dot quantum wells using time-resolved Faraday rotation (TRFR). The spin dynamics shows that the electron  $g$  factor varies as a function of quantum well width and the transverse spin lifetime of several nanoseconds is robust up to room temperature. As a function of probe energy, the amplitude of the TRFR signal shows pronounced resonances, which allow one to identify individual exciton transitions. The resonance energies in the TRFR data are consistent with different exciton transitions in which the electron occupies the conduction-band ground state.

DOI: 10.1103/PhysRevB.71.081309

PACS number(s): 78.67.Hc, 73.22.-f, 78.20.Ls

Nanocrystals have promising applications in optics and spin- or charge-based quantum information schemes because electrons are confined on a nanometer scale. The implementation of quantum information schemes would require several nanocrystals to be assembled into functional structures. For nanocrystals interconnected by conjugated molecules, spin-conserving electron transfer between nanocrystals has been demonstrated.<sup>1</sup> Quantum-dot quantum well (QDQW) heterostructures, where layers of different semiconducting materials alternate in a single nanocrystal, represent an alternative pathway towards the synthesis of functional structures. Both core-shell quantum dots<sup>2-4</sup> and QDQWs (Refs. 5-10) have been synthesized during the past years. QDQWs with a large-bandgap core allow one to investigate quantum confined levels in a geometry in which electrons occupy the surface of a sphere. Both CdS/HgS/CdS (Refs. 6, 7, and 11-13) and CdS/CdSe/CdS (Ref. 10) QDQWs have been well characterized by photoluminescence (PL) and absorption spectroscopy. However, a detailed investigation of the quantum size levels is challenging because of inhomogeneous broadening. Individual exciton transitions have so far only been resolved with techniques such as hole burning, where a subset of homogeneous particles is selected spectroscopically.<sup>7</sup> The electron-spin dynamics in QDQWs has not yet been addressed.

Here, we report time-resolved Faraday rotation (TRFR)<sup>14,15</sup> for CdS/CdSe/CdS QDQWs with varying CdSe quantum well width ( $n_{\text{CdSe}}=1-5$  monolayers). The spin lifetime is on the order of 2-3 ns and almost temperature independent up to 294 K, comparable to CdSe quantum dots.<sup>16</sup> The QDQWs exhibit  $g$  factors that vary with quantum well width. TRFR is not only a unique experimental probe for the spin dynamics, but also a sensitive spectroscopic technique. In contrast to absorption spectra, the amplitude of the TRFR signal as a function of probe energy exhibits several distinct resonances close to the absorption edge, because optical transitions to the lowest conduction-band level are probed selectively. From the level scheme and dielectric-response functions evaluated with  $\mathbf{k}\cdot\mathbf{p}$  calculations,<sup>12,17</sup> we show that the resonance energies in the TRFR data are consistent with the conduction- and valence-band level scheme of spherical

QDQWs. In contrast, the spectral weight of the resonances is not correctly reproduced.

*Experimental results.* Colloidal QDQWs with varying width of the CdSe quantum well were synthesized by a successive ion layer adsorption and reaction (SILAR) technique to produce nanocrystals with accurate control over the quantum well width.<sup>4,10</sup> A schematic representation of the structure is shown in Fig. 1(a). The QDQWs were dissolved in toluene and all measurements were carried out in solution at 294 K unless otherwise specified.

A regeneratively amplified Ti:sapphire laser was used to generate pump and probe pulses of independently tunable wavelength and  $\sim 200$  fs duration through optical parametric amplification. In these measurements, the pump wavelength was fixed at  $\lambda_{\text{pump}}=505$  nm. The pump and probe pulses were both focused to a spot with a diameter of order 100  $\mu\text{m}$  within the QDQW solution. Spin-polarized electrons were excited into the conduction-band states of the QDQWs by the circularly polarized pump pulse. Relaxation of the electron and hole to the lowest exciton state presumably occurs on a picosecond time scale, as in similar systems such as CdS/HgS/CdS QDQWs.<sup>18</sup> The linearly polarized probe pulse then passes through the QDQW solution a time  $\Delta t$  later, where  $\Delta t$  is set using a mechanical delay line in the pump beam path. The Faraday effect causes the polarization of the probe pulse to be rotated by an angle,  $\theta_F$ , proportional to the component of the net spin polarization along the probe beam direction. By recording  $\theta_F$  for varying  $\Delta t$ , we detect the time evolution of the optically injected electron spins in the QDQWs.

Two permanent magnets with adjustable separation were used to apply a magnetic field,  $B_{\text{app}}$ , to the sample perpendicular to the pump and probe direction. Spins that were initially polarized along the pump beam precess around the magnetic field at the Larmor frequency,  $\nu_L=g\mu_B B_{\text{app}}/h$ , where  $g$  is the electron  $g$  factor,  $\mu_B$  the Bohr magneton, and  $h$  the Planck constant. Figure 1(b) shows typical data from a sample with a quantum well width of  $n_{\text{CdSe}}=3$  monolayers and  $B_{\text{app}}=0.3$  T. The inset shows the Fourier transform (FT) power spectrum of the time-domain data. A second precession frequency was observed, as indicated both by the small

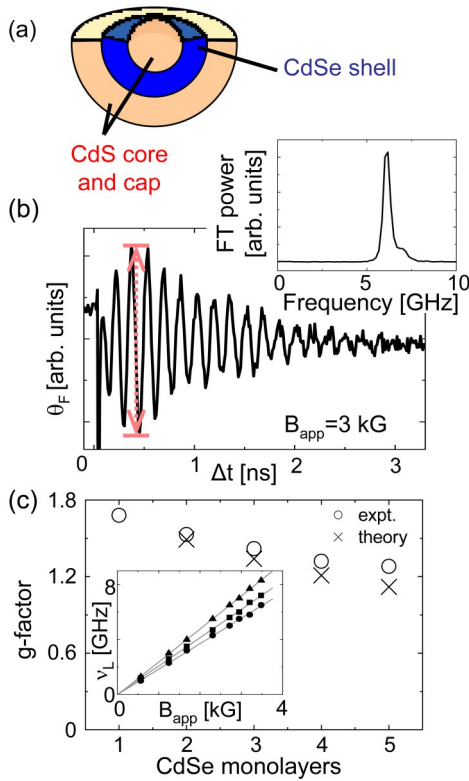


FIG. 1. (Color online) (a) Schematic representation of the QDQW. (b) Typical TRFR data from a QDQW with  $n_{\text{CdSe}}=3$  and  $B_{\text{app}}=3$  kG. The dotted arrow indicates how the amplitude of  $\theta_F$  is determined for Fig. 2. Inset: FT power spectrum of the data. (c) Electron  $g$  factor as a function of CdSe quantum well width. The measured values (circles) are compared to calculated  $g$  factors (crosses). The second  $g$  factor with smaller amplitude is not shown. Inset:  $\nu_L$  as a function of  $B_{\text{app}}$  for  $n_{\text{CdSe}}=1$  (triangles), 3 (squares), and 5 (circles).

shoulder in the FT spectrum and the beating in the time-resolved data. While the origin of this second frequency is unclear in the present case, similar behavior has been observed in CdSe nanocrystals.<sup>15,19–21</sup> There is also a nonoscillating component to the TRFR signal which was also seen in previous measurements on CdSe nanocrystals.<sup>15</sup> In some samples, particularly for  $n_{\text{CdSe}}=5$ , the magnitude of the nonoscillating component is comparable to that of the oscillating component. However, for the purposes of this paper we focus only on the oscillating component [indicated by the arrow in Fig. 1(b)]. The effective transverse spin lifetime,  $T_2^*$ , was of order 2 or 3 ns for all samples measured. The spin lifetime was essentially temperature independent between room temperature and 5 K.<sup>22</sup>

We have performed TRFR measurements as a function of  $B_{\text{app}}$  on samples with CdSe quantum well widths of  $n_{\text{CdSe}}=1–5$  monolayers. In all cases, the results show either one or two precession frequencies that increase linearly with  $B_{\text{app}}$ . The inset of Fig. 1(c) shows the main precession frequency as a function of  $B_{\text{app}}$  for  $n_{\text{CdSe}}=1, 3$ , and 5 monolayers. The measured  $g$  factor for each sample is shown in Fig. 1(c) (circles) in comparison with the theoretical values (crosses) obtained from a weighted average of the CdSe and

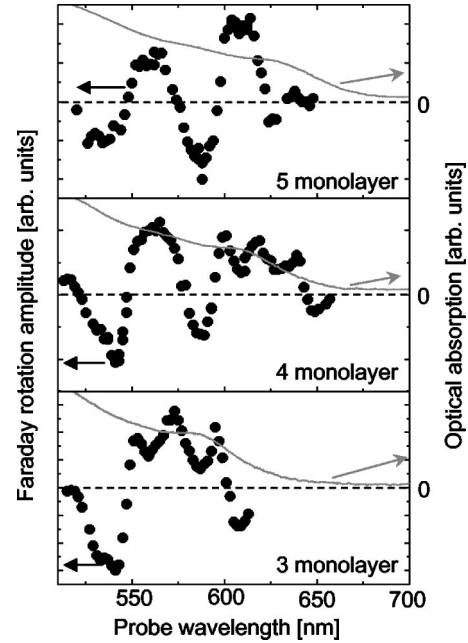


FIG. 2. Amplitude of the Faraday rotation angle,  $\theta_F$ , as a function of probe wavelength for  $n_{\text{CdSe}}=3, 4$ , and 5. The numerical value for  $\theta_F$  was defined as the difference between the local maximum and minimum of the oscillations in the TRFR data nearest to  $\Delta t=500$  ps [Fig. 1(b)], normalized by the probe power. The optical absorption for each sample is also shown.

CdS  $g$  factors (see below). Because of the fairly good agreement, we attribute the observed precession to the electron spin. Within the experimental error, the  $g$  factor did not show any dependence on temperature from 5 K to room temperature<sup>22</sup> or on the probe wavelength.

In order to investigate the QDQW energy levels, we have measured the dependence of the TRFR amplitude on probe wavelength in the samples with  $n_{\text{CdSe}}=3, 4$ , and 5. The probe beam, which had a full width at half maximum of  $\sim 10$  nm, was passed through a monochromator after the sample yielding a wavelength resolution of 2 nm. Figure 2 shows the TRFR oscillation amplitude as a function of probe wavelength for the different samples together with optical absorption data. While the absorption signal only shows a featureless staircaselike behavior with no distinct resonances, the amplitude of the TRFR signal exhibits several pronounced resonances close to the absorption edge. The results in Fig. 2 show that TRFR not only provides information on the spin dynamics, but also is a more sensitive spectroscopic technique than absorption spectroscopy and allows one to identify individual exciton transitions in QDQWs.

*Theoretical description.* We next turn to the theoretical description of the experimental data. The conduction- and valence-band level scheme of spherical QDQWs is calculated with  $\mathbf{k}\cdot\mathbf{p}$  theory,<sup>12,17</sup> using a two-band description for the conduction-band and the four-band Luttinger Hamiltonian in the spherical approximation for the valence band. The conduction-band masses and Luttinger parameters for CdSe and CdS are  $\{m_{\text{CdSe}}/m_0, \gamma_{1,\text{CdSe}}, \gamma_{\text{CdSe}}\} = \{0.11, 1.67, 0.56\}$  and  $\{m_{\text{CdS}}/m_0, \gamma_{1,\text{CdS}}, \gamma_{\text{CdS}}\} = \{0.15, 1.09, 0.34\}$ , respectively, where  $m_0$  denotes the free-electron

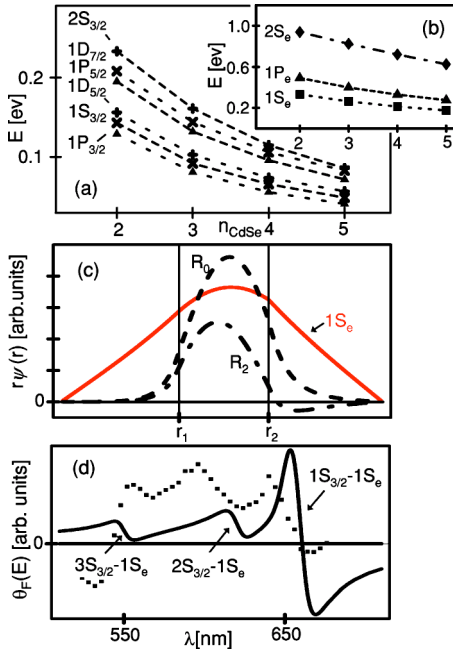


FIG. 3. (Color online) (a) Lowest hole energy levels relative to the CdSe valence-band edge as a function of the quantum well width,  $n_{\text{CdSe}}$ . (b) Conduction-band energy levels relative to the CdSe conduction-band edge as a function of  $n_{\text{CdSe}}$ . (c) Radial wave function of the conduction-band ground state  $1S_e$  (solid) and the  $R_0$  (dashed) and  $R_2$  (dashed-dotted) components of the valence-band state  $1S_{3/2}$  for  $n_{\text{CdSe}}=3$ . (d) Amplitude of the TRFR signal,  $\theta_F(E)$ , calculated from the level schemes in (a) and (b) for a spherical QDQW with  $n_{\text{CdSe}}=3$  and  $\gamma_v=15$  meV (solid line) in comparison with experimental data (symbols).

mass.<sup>23,24</sup> We use the offset of the CdS conduction- and valence-band edge relative to CdSe, 0.32 eV, and 0.42 eV,<sup>25</sup> respectively, to define the radial potential for electrons and holes. The inner and outer radius of the CdSe quantum well is denoted by  $r_1$  and  $r_2$ , respectively. The width of a CdSe monolayer is approximated by the bulk value 0.43 nm (Ref. 26) and the core radius and capping layer width are  $r_1=1.7$  nm and  $r_3-r_2=1.6$  nm, respectively. Details are presented elsewhere.<sup>27</sup>

The energies of the lowest conduction- and valence-band states are shown in Figs. 3(a) and 3(b). Different valence-band multiplets are denoted by  $L_F$ ,<sup>28,29</sup> where  $L$  is the smallest angular momentum of the envelope wave function and  $F$  the total angular momentum. Figure 3(c) shows the radial wave function of the conduction-band ground state  $1S_e$  (solid line) and of  $1S_{3/2}$  (broken lines) for  $n_{\text{CdSe}}=3$ . Because of the larger valence-band mass, the valence-band states are much better localized in the quantum well. The valence-band ground state,  $1P_{3/2}$ , has a  $p$ -type envelope wave function, which is consistent with a dark exciton ground state.

From the energy  $E_{1S_e}$  and wave function  $\psi_{1S_e}(\mathbf{r})$  of the conduction-band ground state  $1S_e$ , the electron  $g$  factor is estimated by a weighted average over the CdSe and CdS  $g$  factors,

$$g = g_{\text{CdSe}} \int_{r_1}^{r_2} d\mathbf{r} |\psi_{1S_e}(\mathbf{r})|^2 + g_{\text{CdS}} \left( \int_0^{r_1} d\mathbf{r} |\psi_{1S_e}(\mathbf{r})|^2 + \int_{r_2}^{r_3} d\mathbf{r} |\psi_{1S_e}(\mathbf{r})|^2 \right). \quad (1)$$

$g_{\text{CdSe}}$  and  $g_{\text{CdS}}$  are given by  $g_{\text{CdSe/CdS}} = 2 - 2E_p \Delta_{\text{so}} / 3(E_g + \Delta_{\text{so}} + E_{1S_e})(E_g + E_{1S_e})$ , where  $E_p$ ,  $E_g$ , and  $\Delta_{\text{so}}$  denote the Kane interband energy, band gap, and spin-orbit energy of CdSe and CdS, respectively. The energy of the conduction-band ground state,  $E_{1S_e}$ , is evaluated relative to the conduction-band minimum. Figure 1(c) shows the theoretical  $g$  values (crosses) obtained with standard parameters for  $E_p$ ,  $E_g$ , and  $\Delta_{\text{so}}$ .<sup>23</sup> The agreement is good for narrow QDQWs, but the theoretical value [Eq. (1)] is smaller than the experimental  $g$  factor for larger  $n_{\text{CdSe}}$ . Possible explanations for this discrepancy are the energy dependence of the conduction-band mass<sup>15</sup> and interface terms in the expression for the  $g$  factor,<sup>30</sup> which are neglected in Eq. (1).

From the calculated single-particle spectrum, we evaluate the amplitude of the TRFR signal as a function of probe energy,  $\theta_F(E)$ , which is proportional to the difference of the dynamic dielectric-response functions for  $\sigma^\pm$  circularly polarized light. The conduction-band electron with  $s_z=1/2$  created by the pump pulse relaxes rapidly to  $1S_e$ , such that  $\theta_F(E)$  is determined by optical transitions to the unoccupied  $1S_e$  state,  $|1S_e; \downarrow\rangle$ ,<sup>31-34</sup>

$$\theta_F(E) = CE \sum_{\sigma=\pm 1; |\Phi_v\rangle} \sigma \langle 1S_e; \downarrow | \hat{p}_x + \sigma i \hat{p}_y | \Phi_v \rangle^2 \times \frac{E - E_{X,v}}{(E - E_{X,v})^2 + \gamma_v^2}. \quad (2)$$

The sum extends over all valence-band states  $|\Phi_v\rangle$ ,  $E_{X,v}$  ( $\gamma_v$ ) denotes the energy (linewidth) of the  $1S_e$ - $\Phi_v$  exciton transition, and  $C$  is a constant. Equation (2) implies that only transitions to the conduction-band ground state contribute to  $\theta_F(E)$ . The transition matrix element is finite for  $S_{3/2}$  valence-band multiplets.<sup>35</sup> Because the characteristic energy splitting between these multiplets is of order 0.1 eV,  $\theta_F(E)$  exhibits several well-defined resonances close to the absorption edge. If the crystal anisotropy is taken into account,<sup>29</sup> these resonances split into doublets, but the characteristic energy splitting is smaller than 25 meV.  $\theta_F(E)$  exhibits distinct resonances for the  $1S_{3/2}$ ,  $2S_{3/2}$ , and  $3S_{3/2}$  multiplets, with a spectral weight that is larger for  $1S_{3/2}$  than for  $2S_{3/2}$  and  $3S_{3/2}$  because of the larger overlap with the envelope wave function of  $1S_e$ . For  $n_{\text{CdSe}}=3$ ,  $\theta_F(E)$  is shown in Fig. 3(d) in comparison with experimental data from Fig. 2. The energies of the  $1S_{3/2}-1S_e$ ,  $2S_{3/2}-1S_e$ , and  $3S_{3/2}-1S_e$  transitions are in good agreement with the experimental resonance energies. We, hence, assign the observed resonances to transitions from the  $1S_{3/2}$ ,  $2S_{3/2}$ , and  $3S_{3/2}$  valence-band multiplets to the conduction-band ground state. For  $n_{\text{CdSe}}=4$  and 5, the agreement with experimental data is comparable, albeit with a somewhat larger discrepancy between the experimental and theoretical resonances ( $\sim 20$  nm).

In contrast to the resonance energies, the spectral weight of the different resonances is not well reproduced by our theory. Possible explanations are the failure of  $\mathbf{k}\cdot\mathbf{p}$  theory, broken spherical symmetry, or a significant variation in the  $nS_{3/2}-1S_e$  exciton linewidth with  $n$ . For the narrow quantum wells with  $n_{\text{CdSe}}=2-5$  studied here, first-principles calculations may be more appropriate than  $\mathbf{k}\cdot\mathbf{p}$  theory for a rigorous description of the QDQW. Broken spherical symmetry leads to a mixing of different valence-band multiplets. The resulting redistribution of the spectral weight from the  $1S_{3/2}-1S_e$  transition to other exciton lines decreases the spectral weight of the ground-state exciton transition.<sup>27</sup> In order to reduce the number of fit parameters in Eq. (2), we have assumed that the linewidths  $\gamma_v$  of all  $nS_{3/2}-1S_e$  exciton transitions are

identical. By allowing for a variation of  $\gamma_v$  with  $n$ , the agreement between experiment and theory in Fig. 3(d) could be further improved.

In conclusion, we have studied the spin dynamics and quantum size levels in QDQWs using TRFR. The variation of the energy levels and the electron  $g$  factor with quantum well width allows one to selectively address quantum wells using optical techniques. Possible future directions include the investigation of the spin and orbital dynamics in more complex heterostructures such as coupled quantum wells.

This work was supported by the ONR and DARPA.

- 
- <sup>1</sup>M. Ouyang and D. D. Awschalom, *Science* **301**, 1074 (2003).  
<sup>2</sup>M. A. Hines and P. Guyot-Sionnest, *J. Phys. Chem.* **100**, 468 (1996).  
<sup>3</sup>B. O. Dabbousi, J. Rodriguez-Viejo, F. V. Mikulec, J. R. Heine, H. Mattoussi, R. Ober, K. F. Jensen, and M. G. Bawendi, *J. Phys. Chem. B* **101**, 9463 (1997).  
<sup>4</sup>J. J. Li, Y. A. Wang, W. Guo, J. C. Keay, T. D. Mishima, M. B. Johnson, and X. Peng, *J. Am. Chem. Soc.* **125**, 12567 (2003).  
<sup>5</sup>A. R. Kortan, R. Hull, R. L. Opila, M. G. Bawendi, M. L. Steigerwald, P. J. Carroll, and L. E. Brus, *J. Am. Chem. Soc.* **112**, 1327 (1990).  
<sup>6</sup>A. Mews, A. Eychmüller, M. Giersig, D. Schooss, and H. Weller, *J. Phys. Chem.* **98**, 934 (1994).  
<sup>7</sup>A. Mews, A. V. Kadavanich, U. Banin, and A. P. Alivisatos, *Phys. Rev. B* **53**, R13 242 (1996).  
<sup>8</sup>Y. C. Tian, T. Newton, N. A. Kotov, D. M. Guldi, and J. H. Fendler, *J. Phys. Chem.* **100**, 8927 (1996).  
<sup>9</sup>R. B. Little, M. A. El-Sayed, G. W. Bryant, and S. Burke, *J. Chem. Phys.* **114**, 1813 (2001).  
<sup>10</sup>D. Battaglia, J. J. Li, Y. Wang, and X. Peng, *Angew. Chem., Int. Ed.* **42**, 5035 (2003).  
<sup>11</sup>D. Schooss, A. Mews, A. Eychmüller, and H. Weller, *Phys. Rev. B* **49**, 17 072 (1994).  
<sup>12</sup>W. Jaskólski and G. W. Bryant, *Phys. Rev. B* **57**, R4237 (1998).  
<sup>13</sup>G. W. Bryant and W. Jaskólski, *Phys. Rev. B* **67**, 205320 (2003).  
<sup>14</sup>J. J. Baumberg, D. D. Awschalom, and N. Samarth, *J. Appl. Phys.* **75**, 6199 (1994).  
<sup>15</sup>J. A. Gupta, D. D. Awschalom, Al. L. Efros, and A. V. Rodina, *Phys. Rev. B* **66**, 125307 (2002).  
<sup>16</sup>J. A. Gupta, D. D. Awschalom, X. Peng, and A. P. Alivisatos, *Phys. Rev. B* **59**, R10 421 (1999).  
<sup>17</sup>E. P. Pokatilov, V. A. Fonoberov, V. M. Fomin, and J. T. Devreese, *Phys. Rev. B* **64**, 245328 (2001).  
<sup>18</sup>M. Braun, C. Burda, M. Mohamed, and M. El-Sayed, *Phys. Rev. B* **64**, 035317 (2001).  
<sup>19</sup>A. V. Rodina, Al. L. Efros and A. Yu. Alekseev, *Phys. Rev. B* **67**, 155312 (2003).  
<sup>20</sup>J. Schrier and K. B. Whaley, *Phys. Rev. B* **67**, 235301 (2003).  
<sup>21</sup>P. Chen and K. B. Whaley, *Phys. Rev. B* **70**, 045311 (2004).  
<sup>22</sup>Low-temperature measurements were performed on QDQWs embedded in an a polyvinyl butyral (PVB) matrix in a magneto-optical cryostat.  
<sup>23</sup>*Semiconductors, II-VI and I-VII Compounds: Semimagnetic Compounds*, edited by U. Rössler, Landolt-Börnstein, New Series, Group III, Vol. 41, Subvolume B (Springer, Heidelberg, 1999).  
<sup>24</sup>T. Richard, P. Lefebvre, H. Mathieu, and J. Allègre, *Phys. Rev. B* **53**, 7287 (1996).  
<sup>25</sup>S.-H. Wei, S. B. Zhang, and A. Zunger, *J. Appl. Phys.* **87**, 1304 (2000).  
<sup>26</sup>J. Li and L.-W. Wang, *Appl. Phys. Lett.* **84**, 3648 (2004).  
<sup>27</sup>F. Meier and D. D. Awschalom, cond-mat/0411429 (unpublished).  
<sup>28</sup>J.-B. Xia, *Phys. Rev. B* **40**, 8500 (1989).  
<sup>29</sup>Al. L. Efros, *Phys. Rev. B* **46**, 7448 (1992).  
<sup>30</sup>A. A. Kiselev, E. L. Ivchenko, and U. Rössler, *Phys. Rev. B* **58**, 16 353 (1998).  
<sup>31</sup>S. Hugonnard-Bruyère, C. Buss, F. Vouilloz, R. Frey, and C. Flytzanis, *Phys. Rev. B* **50**, 2200 (1994).  
<sup>32</sup>N. Linder and L. J. Sham, *Physica E (Amsterdam)* **2**, 412 (1998).  
<sup>33</sup>L. J. Sham, *J. Magn. Magn. Mater.* **200**, 219 (1999).  
<sup>34</sup>F. Meier, V. Cerletti, O. Gywat, D. Loss, and D. D. Awschalom, *Phys. Rev. B* **69**, 195315 (2004).  
<sup>35</sup>A. I. Ekimov, A. A. Onushchenko, A. G. Plyukhin, and Al. L. Efros, *Sov. Phys. JETP* **61**, 891 (1985).